Available online at www.sciencedirect.com
SCIENCE DIRECT
Earth and Planetary Science Letters 243 (2006) 390–399
EPSL
www.elsevier.com/locate/epsl

Reanalysis of ancient eclipse, astronomic and geodetic data: A possible route to resolving the enigma of global sea-level rise

Jerry X. Mitrovica [a,*], John Wahr [b], Isamu Matsuyama [c], Archie Paulson [b], Mark E. Tamisiea [d]

[a] *Department of Physics, University of Toronto, 60 St. George Street, Toronto, Canada M5S 1A7*
[b] *Department of Physics and CIRES, Campus Box 390, University of Colorado, Boulder, CO, 80309, USA*
[c] *Department of Terrestrial Magnetism, Carnegie Institution of Washington, 5241 Broad Branch Road, Washington, DC, 20015, USA*
[d] *Harvard-Smithsonian Center for Astrophysics, 60 Garden Street MS42, Cambridge MA, 02138, USA*

Received 17 August 2005; received in revised form 23 December 2005; accepted 27 December 2005
Available online 15 February 2006
Editor: S. King

Abstract

Predictions of the Earth's response to the ice age appear to simultaneously reconcile a set of astronomical, geodetic and ancient eclipse observations related to changes in rotation, thus ruling out ice melting as a major contributor to 20th century sea-level rise. We demonstrate that the reconciliation disappears when an improved theory of rotational stability is applied. Furthermore, our reanalysis of longer satellite records renders previous estimates of the secular change in rotation rate suspect. The updated ice-age predictions and observations permit an anomalous 20th century ice flux of ~1 mm/yr equivalent sea-level rise. Thus, the full suite of Earth rotation observations are consistent with a connection between climatic warming and recent melting of ice reservoirs.
© 2006 Elsevier B.V. All rights reserved.

Keywords: ancient eclipses; polar wander; Earth rotation; global sea level; glacial rebound

1. Introduction

The potentially strong connection between climate change and global sea-level rise has motivated efforts to constrain the mean amplitude and individual sources of the rise. Direct estimates of the amplitude have come from analyses of tide gauge records which extend, at some sites, several centuries [1], satellite-altimetric data spanning just over one decade [2,3], or combinations of the two data sets [4]. The tide gauge studies suggest a mean 20th century sea-level rise in the range ~1.5–2.0 mm/yr [1,5]. This trend is dominated by a combination of the steric effect of ocean thermal expansion and mass flux from ice reservoirs, including polar ice sheets (Greenland, Antarctica) and small glacier systems. However, despite significant progress toward mapping both ocean heat content [6–8] and the melting of ice complexes, in particular mountain glaciers [9], the detailed partitioning of sea-level change amongst these contributions remains a matter of ongoing debate [10].

The rapid melting of any ice complex yields a distinct geographic pattern in sea-level change [11–14]. This sensitivity suggests a method for analyzing sea-level

* Corresponding author.
E-mail address: jxm@physics.utoronto.ca (J.X. Mitrovica).

0012-821X/$ - see front matter © 2006 Elsevier B.V. All rights reserved.
doi:10.1016/j.epsl.2005.12.029

observations, once they are corrected for the ongoing impact of the last ice age, or glacial isostatic adjustment (GIA), to constrain the individual sources of meltwater. As an example, a so-called fingerprint analysis of GIA-corrected tide gauge records [13] has inferred a mean 20th century mass loss from the Greenland ice complex equivalent to ~0.5 mm/yr of eustatic sea-level (ESL) rise. (We use the term ESL to denote the globally averaged sea-level change that would arise from the meltwater flux into the ocean.) This type of analysis may also be applied to satellite-based constraints on sea-surface changes, but robust estimates will ultimately require the geographic pattern associated with ocean thermal expansion [15].

The redistribution of mass within the Earth system will perturb both the gravitational field of the planet and, via changes in the inertia tensor, the rotation vector. Ongoing GIA, for example, is known to contribute to a broad suite of observations associated with this class of perturbation. These include: astronomical [16,17] measurements of the reorientation of the rotation vector; the accumulated change in the length-of-day over the last three millennia inferred from ancient eclipse records [18]; and space-geodetic [19–21] constraints on secular trends in the spherical harmonic coefficients of the geopotential (the trend in the degree two zonal harmonic, or $\dot{J}_2$, implies a steady redistribution of mass; any such redistribution would cause a linearly proportional trend in the rotation rate [22]). Contemporary melting from global ice reservoirs also implies a mass redistribution, both at the surface and via the associated solid Earth deformation, and this redistribution will contribute to anomalies in the gravitational field and rotational state. Indeed, analyses of various subsets of these observations have, after correction or simultaneous solution for the GIA signal, provided a second method for constraining the amplitude and sources of the non-steric signal in global sea-level rise.

Present-day melting from the Antarctic and Greenland polar ice complexes are almost equally efficient at perturbing the $\dot{J}_2$ observable [23] and thus this long-standing datum [19] provides a potential constraint on the net mass balance within these regions. Efforts to separate these contributions have invoked, in addition to $\dot{J}_2$, observations of a suite of low order zonal harmonics [24,25] (mass fluxes of the same sign in the two high latitude regions yield signals of opposite sign in the odd harmonics [23]), and secular rates of true polar wander (henceforth TPW; off-axis Greenland melting is likely to excite a larger TPW for a given ESL change than melting from the Antarctic) [24,26].

In an influential extension of this philosophy, Munk [27] considered $\dot{J}_2$ (or equivalently the secular change in rotation rate), TPW and ancient eclipse observations, and he described an enigma that serves as the focus of this study. Specifically, Munk argued that estimates of 20th century ocean heat storage are significantly less than required to explain the tide-gauge inferred sea-level rise in terms of ocean thermal expansion. Moreover, the GIA predictions he adopted were able to simultaneously reconcile the three rotation data sets, and this 'triple accord' ruled out significant contemporary melting from global ice reservoirs. Even if the GIA models were tuned so that the $\dot{J}_2$ and TPW observations could accommodate sufficient present-day melting to explain the tide gauge estimates, a consistency between the $\dot{J}_2$ observation and the eclipse data [27] would require roughly that same amount of melting over the last several thousand years, in violation of geological sea-level records [28].

In this paper we revisit the sea-level enigma in light of a new theory [29] for the rotational stability of an ice-age Earth. Furthermore, we propose a route to reconciling the enigma which makes use of a new observational constraint on the $\dot{J}_2$ datum.

2. The sea-level enigma

The 'sea-level enigma' argument is summarized in Fig. 1. The figure shows a comparison of traditional numerical predictions of GIA-induced perturbations in the Earth's rotational state with a suite of observations commonly cited within the GIA literature. The GIA predictions adopt spherically symmetric, self-gravitating, viscoelastic Earth models and a global ice model that is based on the ICE-5G history of Late Pleistocene ice cover [30] (we have also performed calculations using the ICE-3G [31] history and none of the conclusions in the paper are altered by this change.) The Earth models have the elastic and density structure of the seismic model PREM [32], an elastic lithospheric plate of thickness 100 km, an upper mantle viscosity of 10^{21} Pa s, and a uniform lower mantle viscosity (ν_{LM}) that serves as the free parameter of the modelling. The predictions in Fig. 1 are based on standard normal mode theories for GIA-induced perturbations in the Earth's rotational state [22].

GIA predictions of the normalized present-day rate of change of the Earth's axial rotation rate, $\dot{\Omega}/\Omega$, or alternatively the $\dot{J}_2$ datum, exhibit a relatively simple, and well known [22,23,33] sensitivity to variations in ν_{LM} (solid line; Fig. 1A). Models with a weak lower mantle ($\nu_{LM} < 5\times10^{21}$ Pa s) yield small signals because they have relaxed close to equilibrium in the period subsequent to the end of the ice age cycles. Moreover, models with a stiff lower mantle ($\nu_{LM} > 5\times10^{22}$ Pa s) adjust slowly throughout the post-glacial period, and thus also yield relatively small changes in rotation rate.

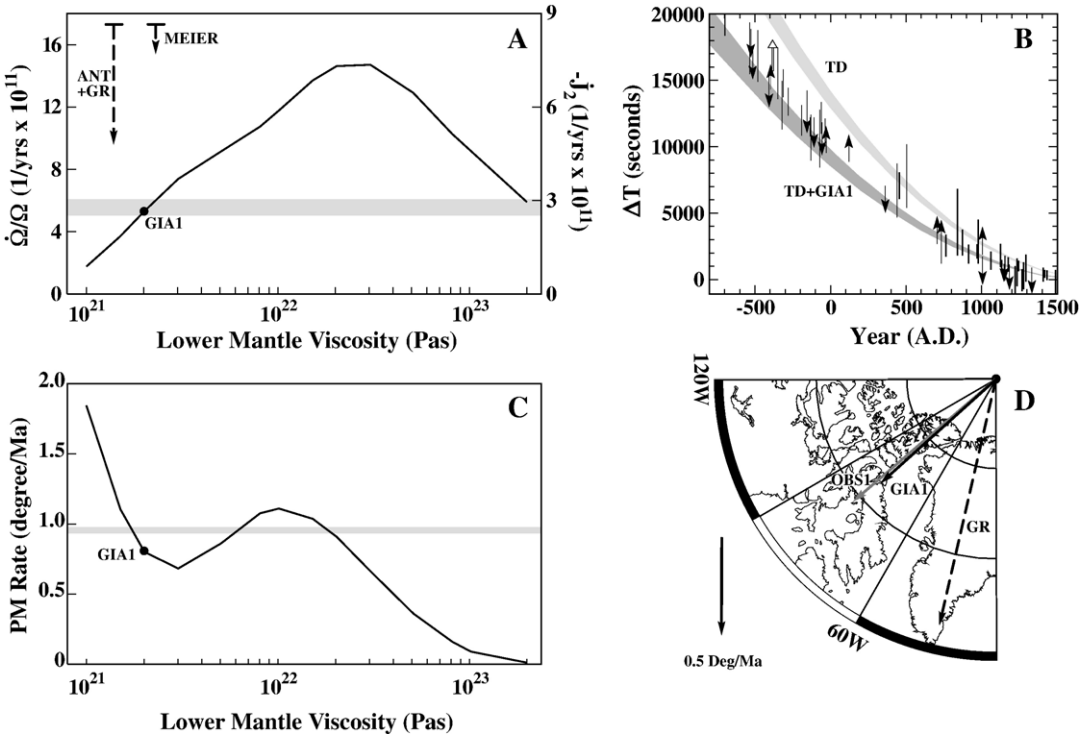

Fig. 1. (A) Solid line — prediction of the GIA-induced present-day rate of change of the Earth's (normalized) axial rate of rotation, $\dot{\Omega}/\Omega$, or the degree two zonal harmonic of the Earth's geopotential, $\dot{J}_2$, as a function of the lower mantle viscosity of the Earth model. The specific result generated from the model GIA1 ($v_{LM}=2\times10^{21}$ Pa s) is labelled. The shaded region represents a satellite-derived observational constraint [21]. The vertical dashed arrows (labelled 'ANT+GR' and 'MEIER') are the predicted magnitudes of the signals associated with a net present-day melting of the Antarctic plus Greenland ice complexes equivalent to a eustatic sea-level rise of 1 mm/yr and Meier's [38] tabulation of mountain glaciers and ice sheets (ESL=0.4 mm/yr), respectively. (B) Vertical lines represent the time difference, ΔT, between the occurrence of individual eclipses and the timing predicted on the basis of the Earth's current rotation rate [18]. These data are obtained from: thin vertical lines — lunar eclipses; thick vertical lines — total solar eclipses; and arrows — partial solar eclipses, where the arrow indicates that the estimate 'extends several thousand seconds' [18]. The small rectangular box with open arrow denotes a recent estimate of ΔT based on a lunar eclipse record from 383BC [50]. The light-shaded region labelled 'TD' is the predicted time difference expected from tidal dissipation under the assumption that dissipation rates have remained fixed to present-day values [18]. The dark shaded zone is the ΔT calculated by combining tidal deceleration with a predicted GIA-induced acceleration of the Earth's rotation, where the latter is based on Earth model GIA1. (C) Predictions of GIA-induced present-day polar wander speed as a function of v_{LM} based on the traditional ice-age rotation theory [22]. The shaded region encompasses observational constraints in two studies [16,17] of astronomical records, and the prediction for model GIA1 is labelled. (D) The observed [17] magnitude and direction of present-day secular polar wander (labelled 'OBS1'), as well as a prediction of the GIA signal based on traditional ice age rotation theory [22] and the viscoelastic model GIA1. The dashed arrow labelled 'GR' represents the motion associated with a net present-day melting of the Greenland ice complex equivalent to a eustatic sea-level rise of 1 mm/yr. The vertical arrow at bottom left of the frame provides a magnitude scale.

Maximum rates are predicted for models that retain significant levels of present-day disequilibrium and adjustment. The shaded region in Fig. 1A represents a constraint on the $\dot{J}_2$ datum ($-2.77\pm0.25\times10^{-11}$ yr^{-1}) inferred from changes in the orbital node rates of the Lageos-1, Lageos-2, Starlette and Ajisai satellites [21]. This constraint is consistent with other satellite laser ranging (SLR) studies [19,20].

Traditional predictions of GIA-induced present-day rates of polar motion [34–37] exhibit a significantly more complex, highly non-monotonic sensitivity to the adopted lower mantle viscosity (solid line; Fig. 1C). In this case, astronomical observations over the last century [16,17] indicate a long-term drift of the rotation pole at a rate of ~1°/Myr (shaded region; Fig. 1C) in the direction of Hudson Bay ('OBS1'; Fig. 1D).

Secular trends in the axial rotation rate (or $\dot{J}_2$) and polar motion represent two planks in the 'enigma' argument against significant recent melting from global ice reservoirs [27]. Munk [27] cites, for example, GIA predictions based on a viscosity inference by Peltier [37] (v_{LM} ~2×10^{21} Pa s; henceforth model GIA1). This model yields predicted present-day GIA signals that are in close accord with observational constraints on the trend in

rotation rate ('GIA1'; Fig. 1A) and both the magnitude (Fig. 1C,D) and direction (Fig. 1D) of polar motion.

The third plank in the enigma argument involves the integrated slowing of the Earth's rotation as inferred from Babylonian, Chinese, Arabic and Greek eclipse observations [18]. The data in Fig. 1B (short vertical lines) represent the total time difference, ΔT, between the recorded occurrence of various eclipses and the predicted time of occurrence under the assumption that the Earth's rotation rate has remained fixed to the present-day value. These data reflect a gradual slowing of the rotation which is largely a consequence of energy dissipation due to ocean tides. Under the assumption that this dissipation has remained constant over the last three millennia, the process would have led to the predicted trend shown by the light-shaded region labelled 'TD' in Fig. 1B [18]. The discrepancy between this trend and the time difference inferred from ancient eclipse records reflects the so-called 'non-tidal acceleration' of the Earth's axial rotation.

Since the end of the last deglaciation phase, the GIA process has been characterized by a gradual reduction in the oblateness of the planet, and hence an acceleration of the Earth's rotation. The time difference associated with GIA can be computed by double integrating (in time) the predicted rate of change in the rotation rate; one integration yields the change in the so-called length-of-day (i.e., the period of rotation) and the second integration provides the accumulated time shift, ΔT. When this integration is applied to predictions based on the model GIA1, the net time difference (TD plus GIA1 prediction) is given by the dark-shaded region in Fig. 1B, which is in agreement with the ancient eclipse observations. Note that a double integration using a constant value of $\dot{\Omega}/\Omega$ equal to the observational constraint in Fig. 1A, $\sim 6\times10^{-11}$ yr^{-1}, provides a similar net time difference, indicating a rough consistency between this datum and the ancient eclipse record [27].

The fit between the GIA1 predictions and observations in Fig. 1A–D defines the 'remarkable' triple accord cited by Munk [27], which 'leaves little room for an eustatic rise in sea level' (p. 6553) from recent melting events. As discussed in the Introduction, melting of either Antarctic or Greenland ice will lead to a similar perturbation in the rotation rate (or $\dot{J}_2$). A net present-day mass flux from these regions equal to an ESL rise of 1 mm/yr yields a predicted slowing of magnitude $\dot{\Omega}/\Omega \sim 8\times10^{-11}$ yr^{-1} (dashed arrow 'ANT+GR'; Fig. 1A) [23]. Furthermore, melting from the suite of mountain glaciers and small ice sheets tabulated by Meier [38] (ESL=0.4 mm/yr) leads to a reduction of $\dot{\Omega}/\Omega \sim 2\times10^{-11}$ yr^{-1} (arrow 'MEIER'; Fig. 1A) [23]. Moreover, off-axis melting of polar ice sheets can have a large impact on polar motion; the results labelled 'GR' in Fig. 1D represent the TPW predicted for melting from Greenland equivalent to an ESL=1 mm/yr. Thus, if the viscoelastic model GIA1, and predictions based upon it, are accurate, any significant recent melting from the polar ice complexes would clearly violate the observational constraints on the secular trend in rotation rate (Fig. 1A) and, if this mass flux involved any non-negligible off-axis contribution (e.g., from Greenland), polar motion (Fig. 1C,D).

As Munk points out, the triple accord evident in Fig. 1 means that the ~1.2 mm/yr of 20th century sea-level rise he infers from tide gauge results after subtracting estimates of the steric contributions remains unaccounted for. Even if one adopts a different GIA model that requires ~1.2 mm/yr of meltwater to match the observed value of $\dot{\Omega}/\Omega$ shown in Fig. 1A, the consistency noted above between this observed value and the eclipse record (Fig. 1B) would imply ~1.2 mm/yr of eustatic sea-level rise during the last three millennia, which would violate geological sea-level records [28].

3. The enigma revisited: a reanalysis of GIA and geodetic data

3.1. GIA and present-day TPW

Is this triple accord robust? To answer this question we consider each datum in turn, beginning with polar motion. The traditional formulation [22] for computing GIA-induced polar wander on viscoelastic Earth models (solid line Fig. 1C; the solid black arrow in 1D) has recently been shown [29] to introduce significant error into these predictions. The physical assumptions underlying the traditional theory, and a newly revised theory [29], are illustrated in Fig. 2A. The GIA-induced reorientation of the rotation vector is governed by a balance between the effects of the surface mass load, which acts to push the rotation pole away (or move the load toward the equator; Fig. 2 A2,A5) and the stabilizing influence of the rotational bulge, which resists excursions of the pole from its initial state. The time-dependent response of the Earth model to both the surface mass loading and the perturbation in the centrifugal potential associated with the polar motion is treated in both the new and traditional formulations using the same, viscoelastic Love number theory [39]. However, these two formulations differ significantly in their treatment of the initial (or background) oblateness of the Earth (compare Fig. 2A1 and A4). Specifically, traditional GIA predictions assume that the background oblateness, which should be connected to the observed ellipticity of the planet, can be accurately

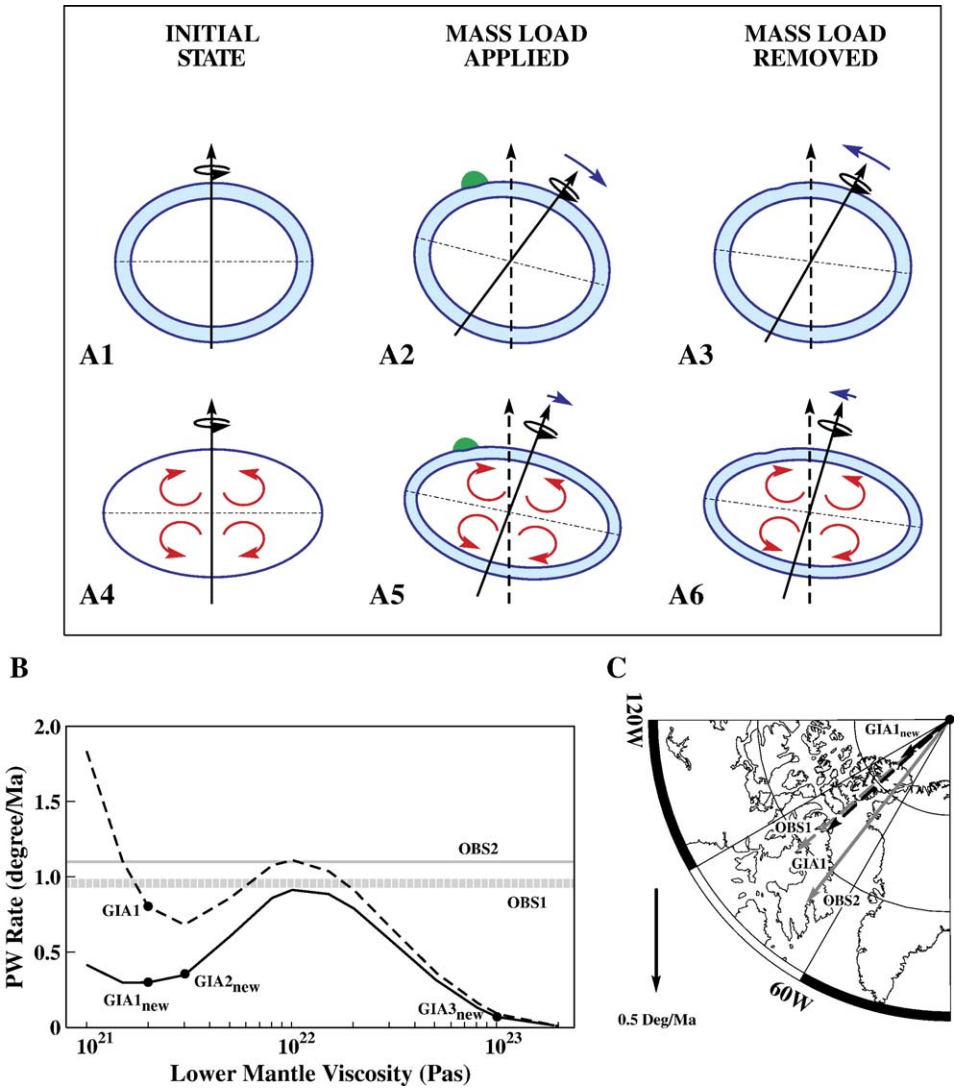

Fig. 2. (A) A schematic illustrating differences between the load-induced perturbation in the orientation of the rotation vector predicted on the basis of traditional GIA rotation theory [22] (top row) and a revised theory [29] that accurately incorporates the magnitude and stabilizing influence of the planetary oblateness (bottom row). The three columns represent, from left, the initial rotational state prior to loading, and the polar motion (shown by blue arrows) during the loading (note the green disk load) and after load removal. In the traditional theory, the initial oblateness is given by the equilibrium form that would result by taking a stationary planet with an elastic lithosphere (given by the blue planetary shell) and introducing an axial rotation equal to the Earth's current rate (frame A1). In the new theory, the oblateness is tied to the observed value and includes the excess ellipticity associated with mantle convection (shown symbolically by the red flow lines). Since the new theory involves a greater background oblateness, it yields a more stable rotation pole; polar motion is thus larger in frames A2 and A3 than A5 and A6. (B) Solid line — as in Fig. 1C, except the predictions of GIA-induced polar wander are generated using the new rotation theory [29]. To simplify comparison, the predictions generated using the old theory [22] are given by the dashed line on the figure (reproduced from Fig. 1C). The subscript 'new' is added to avoid confusion in subsequent discussion. The results $GIA2_{new}$ and $GIA3_{new}$ are described in the text. (C) As in Fig. 1D, except predictions of GIA-induced polar wander amplitude and direction are shown for both the traditional rotation theory (dashed line labelled GIA1, reproduced from Fig. 1D) and the new rotation theory ($GIA1_{new}$). In frames B and C, the observational constraint on polar motion relative to the mean lithosphere frame (OBS1) [17] is reproduced from Fig. 1 and shown by dashed shading. An updated observational constraint on polar motion relative to the hotspot reference frame (OBS2) [41] is given by solid shading.

replaced in the rotation theory by the equilibrium rotating form of the same Earth model used to compute the response to the surface mass loading (Fig. 2A1). This assumption introduces two errors. First, the background oblateness is implicitly, and incorrectly, assumed to be a function of the adopted thickness of the elastic lithosphere (that is, the thicker the blue shell in Fig. 2A1, the smaller the background oblateness adopted in the calculations).

Second, the approach neglects all dynamic (non-GIA) contributions to the observed oblateness, including any excess ellipticity associated with internal, mantle convective flow [40] (shown symbolically by the red flow lines in the bottom frames). A correct formulation [29] avoids these assumptions by connecting, a priori, the background oblateness to the observed flattening of the planet (Fig. 2A4).

The traditional theory thus underestimates the background oblateness and hence the rotational stability of the Earth system in response to the GIA forcing. To quantify this error, we have repeated the calculations shown in Fig. 1C,D using the corrected rotation theory (Fig. 2B,C). (These latter figures also show a newly updated observational constraint [41], labelled 'OBS2', which references the secular polar motion to the hotspot reference frame, rather than the less stable 'mean lithosphere' frame [17]. The new estimate has a magnitude 14% larger than, and a direction 11° counter-clockwise (i.e., toward Greenland) of, the earlier constraint 'OBS1'[17].)

The revised predictions are characterized by significantly lower rates of present-day polar wander. Indeed, the new calculation for model GIA1 (denoted $GIA1_{new}$) is ~65% smaller than the prediction based on the traditional rotation theory, and is now far too small to reconcile the secular trend inferred from astronomical observations (Fig. 2B,C); the triple accord noted by Munk [27] disappears.

3.2. $\dot{J}_2$ Estimates and the 18.6 year tide

Next, we turn to the present-day secular trend in rotation rate, as inferred from observations of $\dot{J}_2$. The revision to the rotation theory outlined in Fig. 2 has no bearing on GIA predictions of $\dot{J}_2$ (or of ΔT). However, a reanalysis of two sets of newly available, monthly, J_2 values inferred from SLR observations, suggests that the commonly cited observational results for $\dot{J}_2$ (Fig. 1A) are more uncertain than previously believed. We refer to these data sets as CC (after Cox and Chao [42]), which runs from 1979 through the fall of 2004, and CT (after Cheng and Tapley [43]), which extends from 1979 through the beginning of 2004. Benjamin et al. [44] used these data to determine a range of values for the amplitude and phase of the 18.6-year body tide. We remove these tidal values from each J_2 data set, and fit a linear trend to the residuals. To test for convergence of our trend solutions, we construct fits over many different time intervals, each beginning in 1979 but ending at times varying between 1994 and the end of the time series. We do this for CC and CT separately, and show the results in Fig. 3A and B. Each panel shows four results, computed by removing different 18.6-year values:

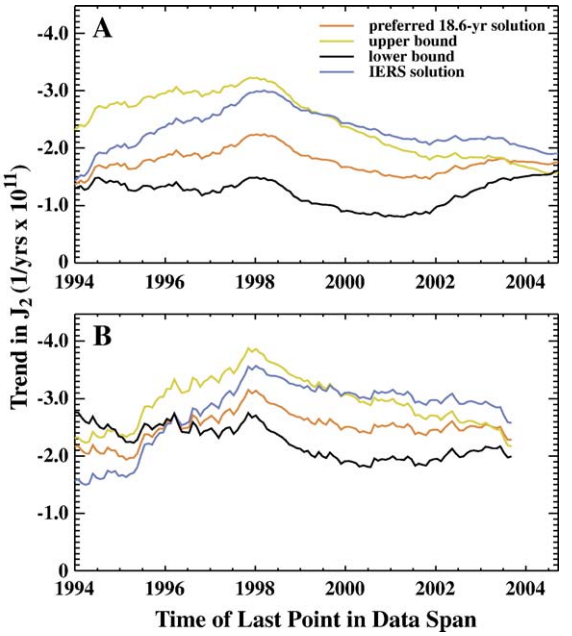

Fig. 3. Results for $\dot{J}_2$ estimated from the monthly J_2 values derived from SLR data by: (A) Cox and Chao [42]; and (B) Cheng and Tapley [43]. The four curves in each panel show results after removing different estimates of the 18.6-year tide from the J_2 values. The preferred solution, and the upper and lower bounds, refer to 18.6-year values inferred by Benjamin et al. [44]. Each point on each curve represents a different time span used for the ΔT; each span starts in 1979 and ends at the time shown on the x-axis. Each curve thus illustrates the degree of convergence of the ΔT.

the upper bound, lower bound, and preferred value from Benjamin et al. [44], and a value which is not based on any 18.6-year tidal observations, but which has been adopted as a standard by the International Earth Rotation Service [45]. Note that the $\dot{J}_2$ results have not yet converged, that they depend on which 18.6-year tide values are removed, and that they are different for CC and CT. The implication is that the SLR data span is still short enough that it is difficult to separate decadal-scale fluctuations from true secular variability. We estimate that the secular trend in J_2 could be anywhere between -1.0×10^{-11} and -3.0×10^{-11} yr^{-1}, a conclusion consistent with the findings of Cox et al. [46]. This corresponds to a range for $\dot{\Omega}/\Omega$ of ~$2–6\times10^{-11}$ yr^{-1} (Fig. 4A).

4. Resolving the enigma? — some examples

One argument which defines Munk's sea-level enigma is that GIA predictions based on models such as GIA1 are able, when coupled with a realistic ice sheet history, to simultaneously satisfy the observational constraints on Earth rotation. A comparison of the revised predictions (solid lines) and updated observations in Figs. 2B and 4A

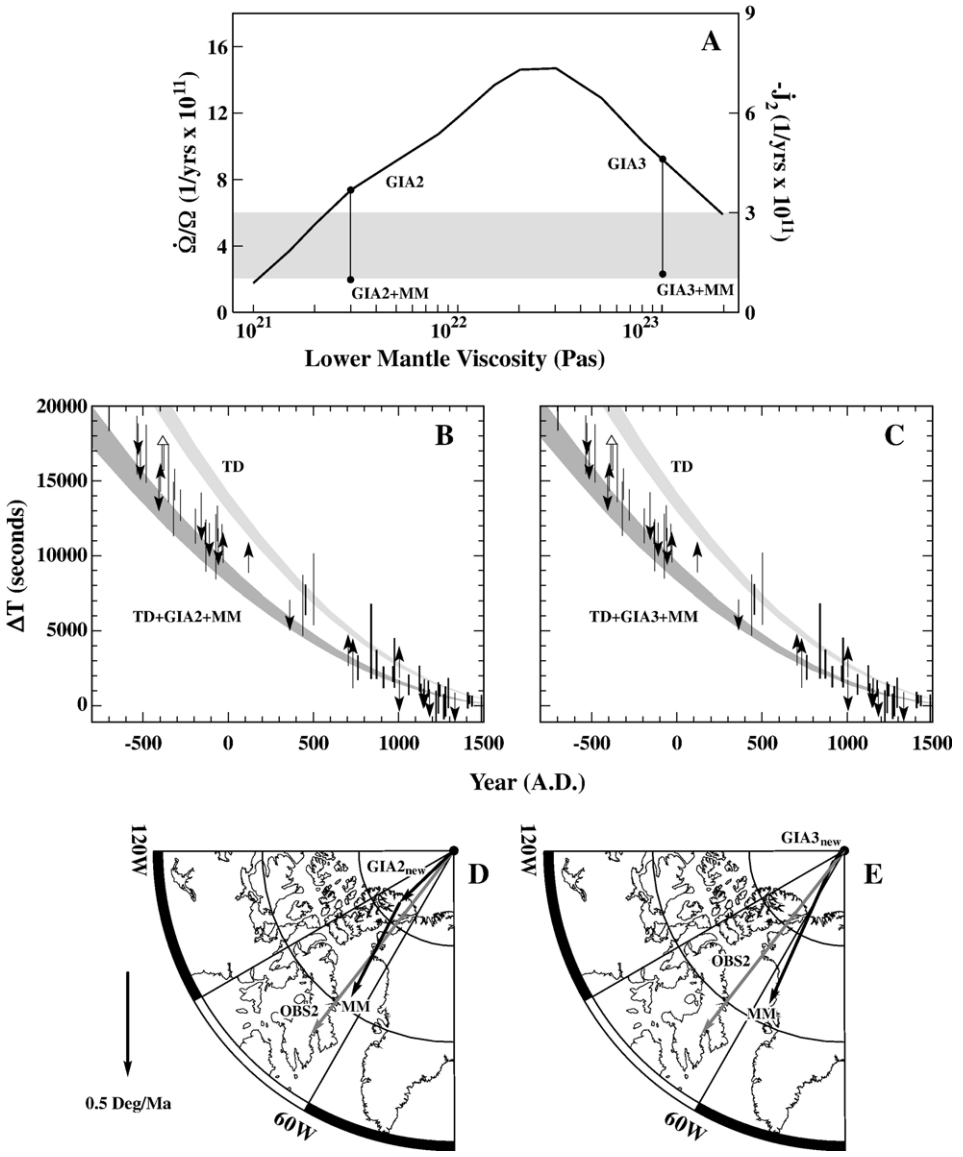

Fig. 4. (A) As in Fig. 1A, a plot of GIA-induced $\dot{J}_2$ and $\dot{\Omega}/\Omega$ as a function of lower mantle viscosity, with an updated observational constraint based on the analysis in Fig. 3. GIA2 and GIA3 refer to results for Earth models with $\nu_{LM}=3\times10^{21}$ Pa s and 10^{23} Pa s, respectively. Also shown is the net perturbation when the GIA predictions for these models are augmented by a signal from post-ice-age melting. This melt model (MM) is comprised of: (1) melting from mountain glaciers and small ice sheets [38] (ESL rise=0.4 mm/yr) and polar ice sheets (ESL=0.4 mm/yr) beginning in the 20th century; (2) Late Holocene melting of polar ice sheets (ESL=0.3 mm/yr). The signal associated with the latter is a function of the lower mantle viscosity (the former is not) and thus the MM signal in Fig. 3 is different for the GIA2 and GIA3 cases. (B,C) As in Fig. 1B, except the results labelled 'TD+GIA2+MM' (frame B) and 'TD+GIA3+MM' (frame C) represent the total time shift, ΔT, predicted from tidal deceleration, and signals from both GIA and the melt history MM. The component of the MM model that involves the onset of melting in the 20th century has negligible effect on these predictions; however, the Late Holocene component of the MM loading (ESL=0.3 mm/yr) contributes a slowing of rotation that is a function of the adopted viscosity model. (D,E) $GIA2_{new}$ (frame D) and $GIA3_{new}$ (frame E) are predictions of the GIA-induced present-day magnitude and direction of polar motion computed using the new rotation theory [29] and viscoelastic models with $\nu_{LM}=3\times10^{21}$ Pa s and 10^{23} Pa s, respectively. In each frame, the vector MM represents the signal associated with the Late Holocene/20th century melt model defined above. In this case, the melting of polar ice sheets is either partitioned evenly between the south Greenland and Antarctic complexes (frames A-GIA2,B,D) or in the ratio 3 : 1 (A-GIA3, C,E).

indicates that no choice of lower mantle viscosity yields a fit to both the $\dot{J}_2$ (or secular trend in rotation rate) and polar motion data. Thus, for the class of GIA models we have explored, which are consistent with those considered by Munk [27], contributions other than GIA must be invoked to reconcile these observations.

As we have discussed, the original constraint on changes in the rotation rate shown in Fig. 1A and the time shift inferred from eclipse records (Fig. 1B) are consistent in the sense that a GIA model that fits one will fit the other (e.g., GIA1 in Fig. 1A,B) [27]. The broader bound on our new, revised estimate of rotation rate changes (or $\dot{J}_2$; Fig. 4A) allows this consistency to be broken, and provides room for a present-day meltwater signal that differs from the 3000-year average. As an example, the maximum discrepancy between the rotation rate change, $\dot{\Omega}/\Omega$, consistent with the eclipse data ($\sim 6\times10^{-11}$ yr^{-1}, see above) and the observational constraint implied by the $\dot{J}_2$ datum ($\sim$2–6×10^{-11} yr^{-1}; Fig. 4A), or $\sim 4\times10^{-11}$ yr^{-1}, permits an increased 20th century meltwater signal from Meier's sources [38] and polar ice sheets of approximately 0.7 mm/yr equivalent ESL rise (see dashed arrows, Fig. 1A). (The minimum discrepancy would, in contrast, return us to a situation where the 20th century value of $\dot{\Omega}/\Omega$ is consistent with the eclipse data, as in Fig. 1A,B, and in this case an increased meltwater signal over the last century would be difficult to accommodate.)

The inferred 3000-year and 20th century averages of melting, rather than the difference between the two, would be a strong function of the adopted GIA model. Once a choice for the uncertain lower mantle viscosity [47] is prescribed, a maximum discrepancy between the GIA prediction and the observed trend in the rotation rate, and thus a maximum signal from ongoing melting, can be established (Fig. 4A). However, the larger the magnitude of the GIA-induced acceleration of rotation, the greater the integrated ΔT due to this process. To retain an acceptable fit to the eclipse records, a fraction of the ongoing melting would have to be extended through the Late Holocene to contribute a slowing of the rotation rate over that period. The partitioning of any ongoing melting between the polar ice complexes can be varied to best-fit the polar motion constraints.

Fig. 4 summarizes the application of this procedure for two example models, GIA2 and GIA3, defined by $\nu_{LM}=3\times10^{21}$ and 10^{23} Pa s, respectively. The predictions are generated by combining GIA calculations based on these models with the signal from a melting model ('MM') defined by: (1) ice mass flux with an onset in the 20th century comprised of melting from Meier's sources [38] ($\dot{\Omega}/\Omega \sim 2\times10^{-11}$ yr^{-1}) and a net retreat of grounded polar ice sheets with an ESL of 0.4 mm/yr ($\dot{\Omega}/\Omega \sim 3.2\times10^{-11}$ yr^{-1}); (2) an additional 0.3 mm/yr of melting from the polar ice sheets during the Late Holocene to the present (note that rotational signals predicted on the basis of the Late Holocene melting component are dependent on the adopted viscosity). The melting of polar ice sheets is either partitioned evenly between the south Greenland and Antarctic complexes (model GIA2 predictions) or in the ratio 3 : 1 (GIA3 predictions). Both scenarios provide a fit to the rotation observations (Fig. 4) which is as good as the GIA1 fit that defined the original sea-level enigma (Fig. 1). Moreover, this fit is obtained with an ongoing melting of global ice reservoirs equivalent to a net ESL rise of 1.1 mm/yr, with 0.8 mm/yr of this total beginning in the 20th century.

This level of Late Holocene melting (0.3 mm/yr) is within the bound inferred on the basis of sea-level records in the far-field of the Late Pleistocene ice complexes by Fleming et al. (see their Fig. 7d) [28]. Moreover, the total rate of Greenland melting ($\sim$0.4 mm/yr for GIA2 and $\sim$0.5 mm/yr for GIA3) is consistent with a fingerprint analysis of modern tide gauge records [13]. As we have discussed, a greater level of ongoing melting would be required if we adopted a viscosity value that yielded a higher residual between the GIA prediction of $\dot{\Omega}/\Omega$ and the observed, e.g, $\nu_{LM}=10^{22}$ Pa s; however, in this case, more of the melting would have to extend through the Late Holocene to reconcile the eclipse record.

5. Final remarks

Our reanalysis of space-geodetic, astronomical and archaeological constraints on Earth rotation has yielded a route to resolving the sea-level enigma discussed by Munk [27]. The GIA models we have considered are incapable of simultaneously reconciling the suite of constraints on the Earth's rotational state. However, for small but plausible values of $\dot{J}_2$, this reconciliation is possible via a combination of GIA and ongoing ice melting of order 1 mm/yr ESL. The details of the melting model MM are not unique, in part because of uncertainties in the deep mantle viscosity and melt geometries, and because it is possible that both polar motion and rotation rate have been significantly impacted by internal Earth processes [48,49]. For example, a non-negligible polar motion signal from mantle convection [48] would alter the inferred partitioning of recent melting between the Greenland and Antarctic ice complexes. Nevertheless, ancient eclipse, modern astronomical and space geodetic constraints on Earth rotation are compatible with a

significant mass loss from global ice reservoirs in response to recent climate change.

Acknowledgement

We thank C. Cox and M.K. Cheng for providing their monthly J_2 estimates, M. Dumberry for providing a copy of his submitted manuscript, Erik Ivins and an anonymous reviewer for their constructive comments, and Andrew M Por for discussions related to this work. We acknowledge support from the Natural Sciences and Engineering Research Council, the Canadian Institute for Advanced Research and the Miller Institute for Basic Research in Science (JXM), NSF grant EAR-0087567 to the University of Colorado (JW, AP), and NASA grant NNG04GF09G (MET).

References

[1] B.C. Douglas, Global sea rise: a redetermination, Surv. Geophys. 18 (1997) 279–292.
[2] A. Cazenave, K. Dominh, M.C. Gennero, B. Ferret, Global mean sea level changes observed by TOPEX-Poseidon and ERS-1, Phys. Chem. Earth 23 (1998) 1069–1075.
[3] R.S. Nerem, G.T. Mitchum, Observations of sea level change from satellite altimetry, in: B.C. Douglas, M.S. Kearney, S.P. Leatherman (Eds.), Sea Level Rise: history and consequences, 2001, pp. 121–163.
[4] J. Church, N. White, R. Coleman, K. Lambeck, J. Mitrovica, Estimates of the regional distribution of sea-level rise over the 1950 to 2000 period, J. Clim. 17 (2004) 2609–2625.
[5] S.J. Holgate, P.L. Woodworth, Evidence for enhanced coastal sea level rise during the 1990s, Geophys. Res. Lett. 31 (2004), doi: 10.1029/2004GL019626.
[6] S. Levitus, J.I. Antonov, T.P. Boyer, C. Stephens, Warming of the world ocean, Science 287 (2000) 2225–2229.
[7] J.I. Antonov, S. Levitus, T.P. Boyer, Thermosteric sea level rise, 1995–2003, Geophys. Res. Lett. 32 (2005), doi: 10.1029/2005GL023112.
[8] J.K. Willis, D. Roemmich, B. Cornuelle, Interannual variability in upper ocean heat content, temperature, and thermosteric expansion on global scales, J. Geophys. Res. 109 (2004), doi: 10.1029/2003JC002260.
[9] M.B. Dyurgerov, M.F. Meier, Glaciers and the changing Earth system: a 2004 snapshot, Institute of Arctic and Alpine Research, Occasional Paper 58 (2005).
[10] A. Cazenave, R.S. Nerem, Present-day sea level change: cbservations and causes, Rev. Geophys. 42, doi: 10.1029/2003RG000139.
[11] R.S. Woodward, On the form and position of mean sea level, U.S. Geol. Surv. Bull. 48 (1888) 87–170.
[12] J.A. Clark, J.A. Primus, Sea-level changes resulting from future retreat of ice sheets: an effect of CO_2 warming of the climate, in: M.J. Tooley, I. Shennan (Eds.), Sea-Level Changes, Institute of British Geographers, London, 1987, pp. 356–370.
[13] J.X. Mitrovica, M.E. Tamisiea, J.L. Davis, G.A. Milne, Polar ice mass variations and the geometry of global sea level change, Nature 409 (2001) 1026–1029.
[14] H.-P. Plag, H.-U. Jüttner, Inversion of global tide gauge data for present-day ice load changes, Proc. 2nd Int. Symp. Environ. Res. Arctic 54 (2001) 301–317.
[15] M.E. Tamisiea, J.X. Mitrovica, G.A. Milne, J.L. Davis, Global geoid and sea level changes due to present-day ice mass fluctuations, J. Geophys. Res. 106 (2001) 30,849–30,863.
[16] D.D. McCarthy, B.J. Luzum, Path of the mean rotation pole from 1899 to 1994, Geophys. J. Int. 125 (1996) 623–629.
[17] R.S. Gross, J. Vondrak, Astrometric and space-geodetic observations of polar wander, Geophys. Res. Lett. 26 (1999) 2085–2088.
[18] F.R. Stephenson, L.V. Morrison, Long-term fluctuations in the Earth's rotation: 700 BC to AD 1990, Philos. Trans. R. Soc. Lond. A 351 (1995) 165–202.
[19] C.F. Yoder, J.G. Williams, J.O. Dickey, B.E. Schutz, R.J. Eanes, B.D. Tapley, $\dot{J}_2$ from LAGEOS and the non-tidal acceleration of Earth rotation, Nature 303 (1983) 757–762.
[20] M.K. Cheng, C.K. Shum, B.D. Tapley, Determination of long-term changes in the Earth's gravity field from satellite laser ranging observations, J. Geophys. Res. 102 (1997) 22377–22390.
[21] R.S. Nerem, S.M. Klosko, Secular variations of the zonal harmonics and polar motion as geophysical constraints, in: R. Rapp, A.A. Cazenave, R.S. Nerem (Eds.), Global Gravity Field and its Variations, IAG Symp. Int. Assoc. of Geod., vol. 116, 1996, pp. 152–163.
[22] P. Wu, W.R. Peltier, Pleistocene deglaciation and the Earth's rotation: a new analysis, Geophys. J. R. Astron. Soc. 76 (1984) 753–791.
[23] J.X. Mitrovica, W.R. Peltier, Present-day secular variations in the zonal harmonics of the Earth's geopotential, J. Geophys. Res. 98 (1993) 4509–4526.
[24] T.S. James, E.R. Ivins, Global geodetic signatures of the Antarctic ice sheet, J. Geophys. Res. 102 (1997) 605–633.
[25] N. Tosi, R. Sabadini, A.M. Marotta, L.L.A. Vermeersen, Simultaneous inversion for the Earth's mantle viscosity and ice mass imbalance in Antarctica and Greenland, J. Geophys. Res. 110 (2005), doi: 10.1029/2004JB003236.
[26] P. Johnston, K. Lambeck, Postglacial rebound and sea level contributions to changes in the geoid and the Earth's rotation axis, Geophys. J. Int. 136 (1999) 537–558.
[27] W. Munk, Twentieth century sea level: an enigma, Proc. Natl. Acad. Sci. 99 (2002) 6550–6555.
[28] K. Fleming, P. Johnston, D. Zwartz, Y. Yokoyama, K. Lambeck, J. Chappell, Refining the eustatic sea-level curve since the Last Glacial Maximum using farand intermediate-field sites, Earth Planet. Sci. Lett. 163 (1998) 327–342.
[29] J.X. Mitrovica, J. Wahr, I. Matsuyama, A. Paulson, The rotational stability of an ice age Earth, Geophys. J. Int. 161 (2005) 491–506.
[30] W.R. Peltier, Global glacial isostasy and the surface of the ice-age Earth: the ICE-5G (VM2) Model and GRACE, Annu. Rev. Earth Planet. Sci. 32 (2003) 111–149.
[31] A.M. Tushingham, W.R. Peltier, ICE-3G: a new global model of late Pleistocene deglaciation based upon geophysical predictions of postglacial relative sea level change, J. Geophys. Res. 96 (1991) 4497–4523.
[32] A.M. Dziewonski, D.L. Anderson, Preliminary reference Earth model (PREM), Phys. Earth Planet. Int. 25 (1981) 297–356.
[33] E.R. Ivins, C.G. Sammis, C.F. Yoder, Deep mantle viscous structure with prior estimate and satellite constraint, J. Geophys. Res. 98 (1993) 4579–4609.

[34] D.A. Yuen, R. Sabadini, E.V. Boschi, Viscosity of the lower mantle as inferred from rotational data, J. Geophys. Res. 87 (1982) 10745–10762.
[35] G.A. Milne, J.X. Mitrovica, Postglacial sea-level change on a rotating Earth: first results from a gravitationally self-consistent sea-level equation, Geophys. J. Int. 126 (1996) F13–F20.
[36] W.R. Peltier, X. Jiang, Glacial isostatic adjustment and Earth rotation: re-fined constraints on the viscosity of the deep mantle (correction), J. Geophys. Res. 102 (1997) 10101–10103.
[37] W.R. Peltier, Postglacial variations in the level of the sea: implications for climate dynamics and solid-Earth geophysics, Rev. Geophys. 36 (1998) 603–689.
[38] M.F. Meier, Contribution of small glaciers to global sea level, Science 226 (1984) 1418–1421.
[39] W.R. Peltier, The impulse response of a Maxwell Earth, Rev. Geophys. Space Phys. 12 (1974) 649–669.
[40] S.M. Nakiboglu, Hydrostatic theory of the Earth and its mechanical implications, Phys. Earth Planet. Int. 28 (1982) 302–311.
[41] D.F. Argus, R.S. Gross, An estimate of motion between the spin axis and the hotspots over the past century, Geophys. Res. Lett. 31 (2004), doi: 10.1029/2004GL019657.
[42] C.M. Cox, B.F. Chao, Detection of a large-scale mass redistribution in the terrestrial system since 1998, Science 297 (2002) 831–832.
[43] M. Cheng, B.D. Tapley, Variations in the Earth's oblateness during the past 28 years, J. Geophys. Res. 109 (2004) B09402.
[44] D. Benjamin, J. Wahr, R. Ray, G. Egbert, S.D. Desai, Constraints on mantle anelasticity from geodetic observations, and implications for the J_2 anomaly, Geophys. J. Int., (in press).
[45] D.D. McCarthy, G. Petit (Eds.), IERS Conventions (2003), International Earth Rotation and Reference Service (IERS) Technical Note No. 32, 2004.
[46] C.M. Cox, A. Boy, B.F. Chao, Time-variable gravity: using satellite-laser-ranging as a tool for observing long-term changes in the earth system, in: R. Noomen, S. Klosko, C. Noll, M. Pearlman (Eds.), Proceed. 13th Int. Workshop on Laser Ranging, NASA/CP-2003-212248, 2003, pp. 9–19.
[47] J.X. Mitrovica, Haskell [1935] revisited, J. Geophys. Res. 101 (1996) 555–569.
[48] B. Steinberger, R.J. O'Connell, Changes of the Earth's rotation axis owing to advection of mantle density heterogeneities, Nature 387 (1997) 169–173.
[49] M. Dumberry, J. Bloxham, Azimuthal flows in the Earth's core and changes in length of day at millennial timescales, Geophys. J. Int., (in press).
[50] J.M. Steele, Ptolemy, Babylon and the rotation of the Earth, Astron. Geophys. 46 (2005) 5.11–5.15.